



Effects of tube shape on the distribution of film thickness and heat transfer performance in falling film evaporation

Huanhao Zhang¹ · Yasu Zhou¹

Received: 23 June 2021 / Accepted: 28 February 2022 / Published online: 15 March 2022
© The Author(s), under exclusive licence to Springer-Verlag GmbH Germany, part of Springer Nature 2022

Abstract

The evaporative condenser has broad application prospects because of its high heat transfer efficiency. In order to explore the effect of tube shape on the film thickness and heat transfer performance of evaporative condenser. In this study, 2-D computational models of different tube shapes were built to simulate the flow behavior and heat transfer characteristics of falling film, and the reliability validation on simulation data was performed by the comparison of experimental value. The model contains one round tube and four half-oval tubes, and the five tubes have a equality of perimeter. The liquid film distribution, heat transfer coefficient and dimensionless temperature were calculated and analysed, respectively. It concluded that the water film gets thinner and thinner with the tube shape becoming narrow and long, and the average liquid film thickness of four half-oval tubes are about 3.7–11.4% lesser than that of round tube. Furthermore, the dimensionless temperature of the half-oval tubes is smaller in contrast with round tube, which indicates a larger heat transfer coefficient. The mean heat transfer coefficient of the four half-oval tubes nearly increased by 3.2%, 6.5%, 8.7% and 11.3% on the basis of round tube, respectively.

Nomenclature

a	Long half axis of the ellipse, mm
b	Short half axis of the ellipse, mm
coeff	Mass transfer coefficient, s^{-1}
d	Distance from tube surface to a point in the liquid film, mm
D	Diameter, mm
E	Internal energy, J/kg
f	The component force of gravity, N
F_{vol}	The surface tension force
g	Gravitational acceleration, m/s^2
G	Gravity, N
H	Specific enthalpy, J/kg
h	Local heat transfer coefficient, $kw/(m^2 \cdot K)$
l	Half circumference of the tube, mm
m	Mass of phase transfer, $kg/(m^3 \cdot s)$
p	Pressure, Pa
q	Heat flux, kw/m^2
Re	Reynolds number
T	Temperature, K
u	Velocity scale in x direction
v	Velocity scale in y direction

x	Arc length, mm
X	Circumferential dimensionless location, $= x/l$, ($0 \leq X \leq 1$)

Greek symbols

α	Volume fraction, %
κ	Interface curvature, 1/m
μ	Dynamic viscosity, $kg/(m \cdot s)$
ρ	Density, kg/m^3
λ	Thermal conductivity, $w/(m \cdot K)$
σ	Surface tension coefficient, N/m
ν	Kinematic viscosity, m^2/s
φ	Circumferential angel
θ	Dimensionless temperature, $\theta = (T_l - T_i)/(T_w - T_i)$, ($0 \leq \theta \leq 1$)
δ	Liquid film thickness, mm
η	Dimensionless film thickness, $\eta = d\delta$
ε	$\varepsilon = B/a$
Γ	Spray density, $kg/(m \cdot s)$

Subscripts

ave	Average
i	Inlet of water
g	Gas
l	Liquid
sat	Saturation
w	Wall

✉ Yasu Zhou
zhouys@dhu.edu.cn

¹ College of Environmental Science and Engineering,
Donghua University, Shanghai 201620, China

1 Introduction

Falling-film technique has a large number of applications, such as evaporative condenser, wet cooling tower, and other process of heat and mass transfer [1–3] due to the merit of high energy efficiency and water conservation [4, 5]. In a falling film evaporation system, the water drop to the top of the tube surface from the spray nozzles, and then cover the tube wall, forming a water film finally. The heat and mass transfer efficiency is greatly affected by flow characteristics over the horizontal tube. The thicker film thickness means a higher thermal resistance, which is bad for the heat transfer. Thus, falling film evaporation that has important meaning and potential value on energy saving is worthy to further investigate.

So far significant headway of flow characteristic in falling-film evaporation has been performed. Nusselt [6] first put forward the theory of falling film and presented a classical empirical formula for the two-dimensional film thickness under sheet flow.

$$\delta = \left(\frac{3\mu_l \Gamma}{\rho_l(\rho_l - \rho_g) \sin \varphi} \right)^{1/3} \quad (1)$$

With above definition, the Reynolds number was given as follow:

$$Re = \frac{4\Gamma}{\mu_l} \quad (2)$$

Lin et al. [7] simulated the liquid film distribution and heat transfer coefficient for three circular tubes with different diameter under the condition of Reynolds number varying from 368 to 800, and showed that the influence of Reynolds number on the two parameters is larger than the tube diameter. Chen et al. [8] utilized laser-induced fluorescence method to measure water and seawater liquid film thickness outside circular tubes, they found that there is no obvious difference in liquid film thickness between the two fluid. Hou et al. [9] gauged the water film thickness outside circular tube bundles with a displacement micrometer, and based on Nusselt correlation, developed a new expression for film thickness of which the tube diameter and pitch were taken into account. Xu et al. [10] conducted a measurement for film thickness over round tubes with the JDC-II device, and presented a empirical expression to predict the fluctuation intensity of falling film in the case of different Reynolds number. Zhang et al. [11] performed an experiment to research the film thickness distribution outside a corrugated tube, which revealed that the dryout phenomenon barely appears on the tube surface due to the special structure of the tube. Gstoehl et al. [12] measured the film thickness for water, water–glycol mixture, ethylene glycol three kinds of fluid outside a horizontal

circular tube, which showed that Nusselt falling film theory agrees well before the 90° circumference angle, however has some deviation when the circumference angle is larger than 90°. Zhou et al. [13] built a 3D model to research the falling film thickness over the round tube wall, they pointed out film thickness increases as Reynolds number increasing, while dry spot at the bottom of the tube also increases at same time. Wang et al. [14] derived expressions of liquid film thickness for different flow region under column flow with a 3D model. Qiu et al. [15] studied the film thickness distribution of different fluid on the wall of horizontal tube, they showed that liquid viscosity is the major factor that leads to the different jet flow. Qiu et al. [16] used a three dimensional model to study flow characteristics of one and two liquid column around a horizontal tube, they concluded that the falling film of one liquid column has a uniform distribution, in contrast, the falling film of two liquid column forms a uplift due to collision of liquid film. Yan et al. [17] adopted a high-speed camera and IC measure method to implement a measurement of water film thickness over a round tube, they concluded that the nozzles-holes configurations is a key factor for the distribution of falling film. Li et al. [18] developed a 3D model to study water film distribution over round tube surface under the influence of counter-current wind speed, and found the location of thinnest film thickness will move upward along the perimeter direction when wind is imposed in the case of droplet and column flow condition. Parken et al. [19] implemented a experiment on heat transfer performance of evaporation and boiling around horizontal brass tubes, the mean heat transfer coefficient were calculated and analysed, finally, the expressions of mean heat transfer coefficient to different evaporation process were presented. Pu et al. [20] simulated the flow and heat transfer process for falling film over flat tubes with a 2D model, the result revealed heat transfer coefficient increases as tube shape of flat tubes get narrow and long. Li et al. [21]. conducted an experiment to research falling film evaporation of three enhanced tube and a smooth tube in the condition of small Reynolds number and convective evaporation, which derived heat transfer performance over tube with enhanced inner surface is better than that of smooth tube. Qi et al. [22] studied the heat transfer coefficient around different tube shape with seawater as working fluid, it found that the elliptical tube is about 20–25% higher than circular tube. Ji et al. [23] experimentally study heat transfer performance of R134a that evaporate in the form of liquid film under the action of gas velocity, they showed that the larger gas velocity is beneficial to the uppermost two tubes. Zhao et al. [24] simulated the liquid film distribution in circumferential direction over a round tube, they point out that surface tension has a great influence on the flow behavior of liquid film, then derived expressions of liquid film thickness for different range of circumferential angle.

It can be learned from the literature survey above that most previous researches pay attention to circular tube, but few studies focused on non-circular tube in the area of falling film evaporation. Pu et al. [20] and Qi et al. [22] have proved that the special tubes possess a better heat transfer performance than round tube in the area of desalination. Nowadays, the round tubes dominate in evaporative condenser, the superiority of non-circular tubes has not been appreciated. It is believed that gravity component of half-oval tube in flow direction is larger than round tube. So leads to a higher velocity of falling film, which means a thinner water film thickness compared with circular tube. Thus, more details and extensive studies are needed to model horizontal falling film behaviour of half-oval tubes and clarify the mechanisms of flow enhancement. In other words, half-oval tube is beneficial to the heat transfer for falling film technique. Therefore it is necessary to investigate the performance that liquid film evaporates over half-oval tube.

The primary objective of this paper is to state that half-oval tube has superiority in contrast with round tube in the process of falling evaporation. The falling film distribution and heat transfer coefficient were calculated. A test rig was built to verify the simulation data of liquid film thickness, moreover by comparison of the experiment value of previous literature, the reasonability of heat transfer coefficient was also demonstrated. The simulation data manifest good consistency with the values of experiment, which indicates the reliability of the model. In addition, the dimensionless temperature inside liquid film at different circumferential dimensionless location are calculated to reveal the distribution of thermal boundary layer around circular and half-oval tubes.

2 Numerical model

2.1 The geometric parameters of two kinds of tube

As shown in Fig. 1, the half-oval tube is formed by an upper semicircle and a lower half ellipse, In this paper, the half-oval

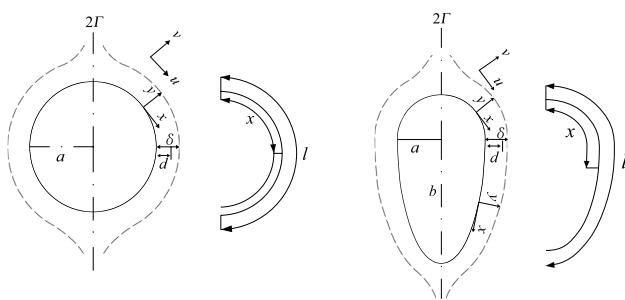


Fig. 1 Schematic diagram of circular and half-oval tube

tube ($\epsilon = 3.2$) was selected as benchmark, then make sure that the perimeter is same and change the ratio of b to a to attain the circular tube and the other 3 half-oval tubes. The tubes parameters are listed in Table 1. The ratio of b to a is defined as ϵ . That is to say, the half-oval tube becomes narrow and long as ϵ increases, so the gravity component in perimeter direction gets larger.

2.2 Computational model and governing equations

The software of FLUENT 16.0 is used to conduct the simulation. VOF model is a surface tracking method under fixed Euler grid, which can obtain the interface of two or more incompatible fluids. So the VOF model is utilized to simulate the two-phase flow because it can accurately extract the edge of water film compared with other multiphase flow model. The gas-liquid interface can be identified by the water volume fraction of 0.5. The range of volume fraction is 0 to 1, and the volume fraction of all the phases adds up to 1. The volume fraction of 1 indicates that a grid cell is filled with liquid or gas, therefore there is no other phase in that grid. Water vapor is set to the first phase due to the small density, so water liquid is the secondary phase.

The continuity equation of VOF model is written as:

$$\frac{\partial u_x}{\partial x} + \frac{\partial u_y}{\partial y} = 0 \tag{3}$$

The continuity equation of secondary phase is as follows:

$$\frac{\partial}{\partial t} (\alpha_w \rho_w) + \nabla \cdot (\alpha_w \rho_w \vec{u}_w) = S_m \tag{4}$$

Momentum equation:

$$\frac{\partial(\rho \vec{u})}{\partial t} + \nabla \cdot (\rho \vec{u} \vec{u}) = \nabla \left[\mu (\nabla \vec{u} + \nabla \vec{u}^T) \right] - \nabla p + \rho \vec{g} + F_{vol} \tag{5}$$

Energy equation:

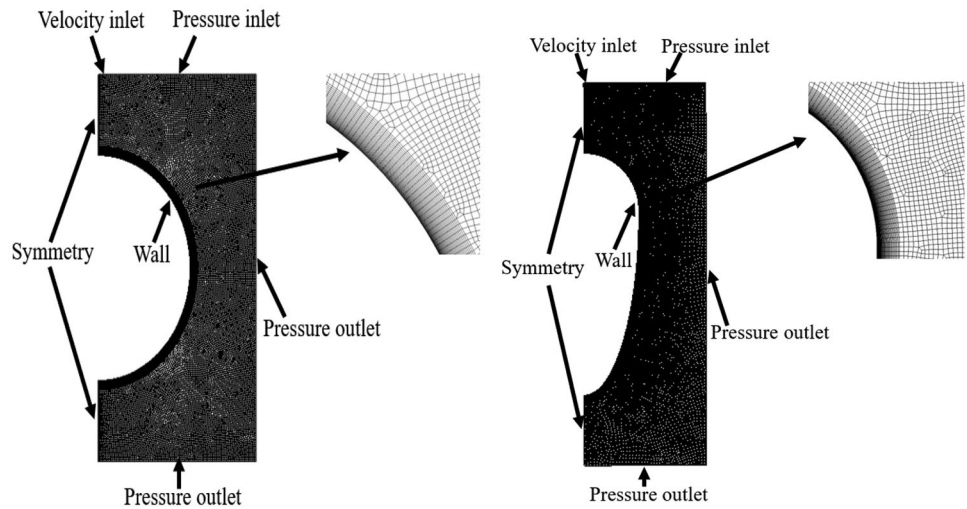
$$\frac{\partial(\rho E)}{\partial t} + \nabla \cdot (\rho E \vec{u}) = \nabla \cdot (k \cdot \nabla T) + \nabla \cdot (\rho \vec{u}) + S_e \tag{6}$$

Evaporation scheme.

Table 1 Tube type parameters

Number	Tube type	$\epsilon(b/a)$	b (mm)	a (mm)
A	Circular tube	1	13.93	13.93
B	Half-oval tube 1	2	21.14	10.57
C	Half-oval tube 2	3.2	26.20	8.20
D	Half-oval tube 3	4	28.52	7.13
E	Half-oval tube 4	5	30.65	6.13

Fig. 2 Mesh structure and boundary conditions



Heat and mass transfer process for gas liquid phase is calculated by Lee model according to previous paper [7]. In order to use Lee model, the continuity equation need to be amended.

$$\frac{\partial}{\partial t}(\alpha_g \rho_g) + \nabla \cdot (\alpha_g \rho_g \vec{u}_g) = m_{lg} - m_{lw} \tag{7}$$

In Lee model, the evaporation process that water evaporates into vapor occurs if water temperature is larger than T_{sat} . In contrast, the counterpart process is condensation that gas condenses into liquid. The above two process was described by the following equations:

$$m_{lg} = -coeff \cdot \alpha_w \rho_w \frac{T_l - T_{sat}}{T_{sat}} T_l > T_{sat} \tag{8}$$

$$S_e = -coeff \cdot \alpha_w \rho_w \frac{T_l - T_{sat}}{T_{sat}} H \tag{9}$$

$$m_{gl} = coeff \cdot \alpha_g \rho_g \frac{T_{sat} - T_g}{T_{sat}} T_g < T_{sat} \tag{10}$$

$$S_e = coeff \cdot \alpha_g \rho_g \frac{T_{sat} - T_g}{T_{sat}} H \tag{11}$$

where $\nabla = \frac{\partial}{\partial x} \vec{i} + \frac{\partial}{\partial y} \vec{j} + \frac{\partial}{\partial z} \vec{k}$, *coeff* is set as 0.1 based on the literature [25].

The continuum surface force scheme presented by Brackbill [26] was used to calculate the surface tension of liquid film. The source term of surface tension which is in the momentum equation can be calculated using the following expression.

$$F_{vol} = \sigma k \nabla \alpha \tag{12}$$

The thermophysical parameters of mixture can be obtained by adding the product of volume fraction α and parameters of each phase:

$$\rho = (1 - \alpha_l) \rho_g + \alpha_l \rho_l \tag{13}$$

$$\mu = (1 - \alpha_l) \mu_g + \alpha_l \mu_l \tag{14}$$

$$E = \frac{(1 - \alpha_l) \rho_g E_g + \alpha_l \rho_l E_l}{(1 - \alpha_l) \rho_g + \alpha_l \rho_l} \tag{15}$$

$$\alpha_l + \alpha_g = 1 \tag{16}$$

Local and mean heat transfer coefficient are described below:

$$h = \frac{q}{T_w - T_i} \tag{17}$$

$$h_{ave} = \frac{1}{l} \int_0^l h dx \tag{18}$$

2.3 The grid model and boundary conditions

The boundary layer mesh was used to improve the quality of mesh, The thickness of first layer mesh next to the tube surface is 0.01 mm, which can extract liquid film thickness

Table 2 Physical property parameters

Physical parameter	Water liquid	Water vapor
Density, kg/m ³	997	0.0231
Viscosity, kg/(m · s)	8.94e-04	9.87e-06
Surface Tension, N/m	0.072	'
Specific heat kJ/(kg · K)	4.183	1.878
Thermal conductivity, W/(m · K)	0.595	0.0186

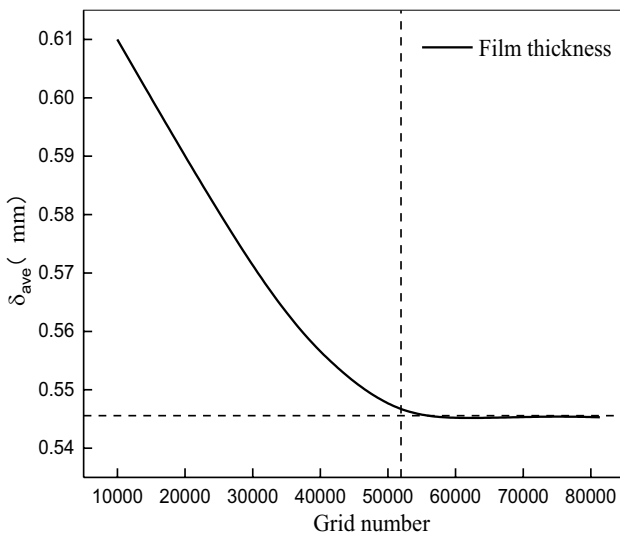


Fig. 3 Grid independence verification ($\epsilon = 3.2$, $Re = 1104$)

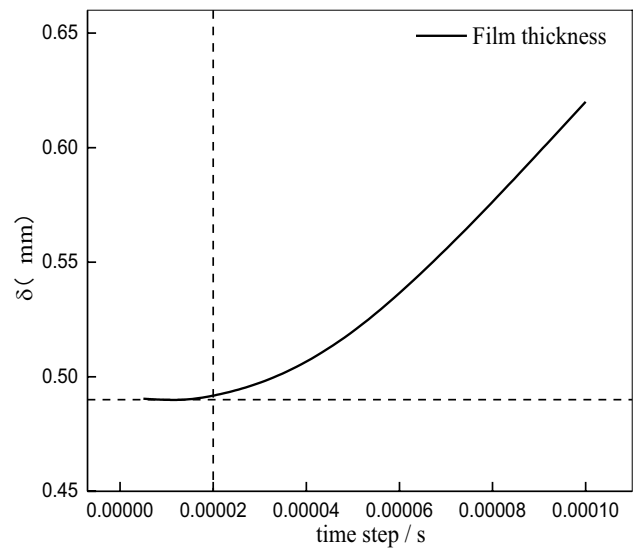


Fig. 4 Verification of time step independence ($\epsilon = 3.2$, $Re = 1104$, $X = 0.5$)

accurately. As illustrated in Fig. 2, velocity inlet and pressure inlet are in the top area. The volume fraction of water in velocity inlet is set to 1. The width of water inlet is 1 mm with a spray height of 10 mm. The inlet water temperature and the saturation temperature are 298.15 K and 303.15 K respectively. The tube surface is stationary wall boundary condition and the heat flux to wall is 30 Kw. The left side is defined as symmetry boundary condition, and the remaining two brim are pressure outlet.

2.4 Fluid properties and assumptions

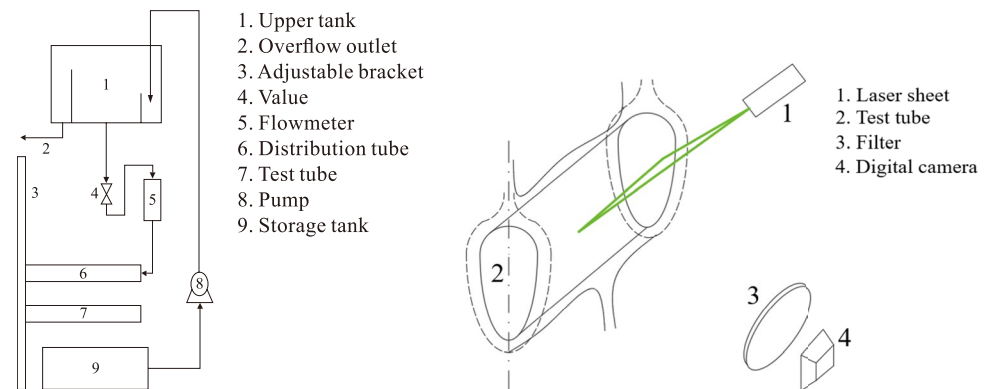
The Reynolds number range for the transition from laminar to turbulent flow is 4000 to 6000 [27], which means that the flow is laminar if the Reynolds number is less than 4000. The Reynolds number range of this study is 938 to 1430, so the flow is considered to be laminar.

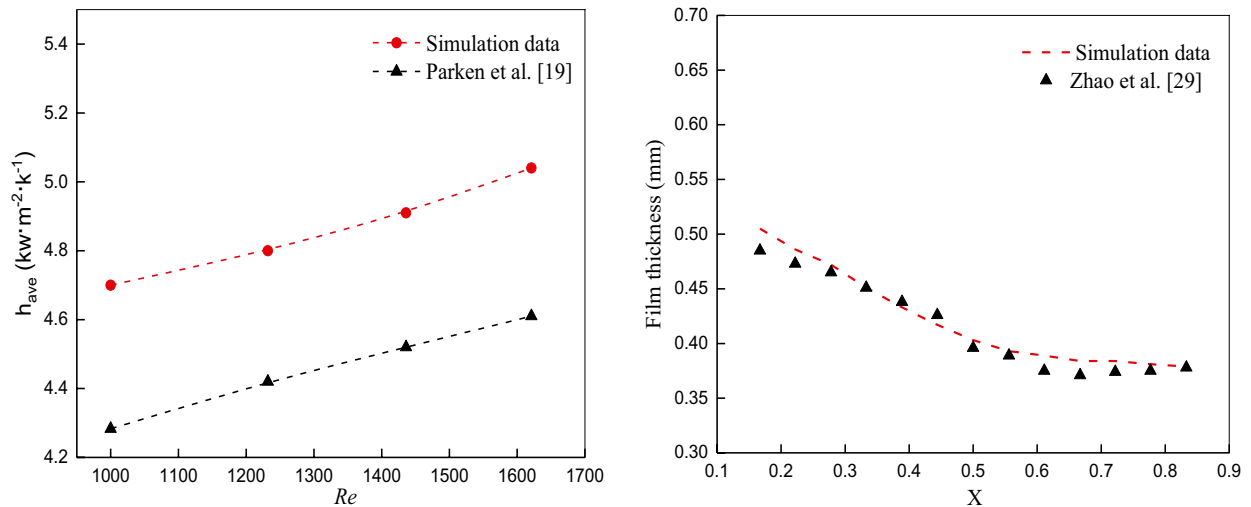
Reasonable simplification can consider the major factors and ignore the minor ones to accelerate the computational rate under the premise that simulation result is close to the experimental value. For the purpose of simplifying the simulation process, some assumptions are given as follows: (a) The contact angel is set to 0° , (b) Liquid water is incompressible. (c) The operating condition is considered as adiabatic. (d) Pressure is constant in the computational domain. (e) No properties difference of fluid exits in the simulation process. Table 2 display the parameters of two fluid.

2.5 Mesh independence

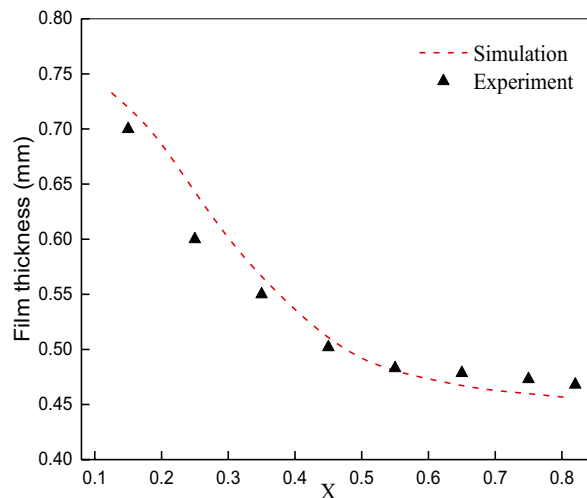
The mesh density is a decisive factor for the result of simulation. An appropriate mesh density can not only ensure the accuracy of simulation results but also reduce the simulation

Fig. 5 Schematic diagram of experimental apparatus and image sampling





(a) Mean heat transfer coefficient ($D = 25.4$ mm) (b) Falling film thickness in circumferential direction ($D = 25.4$ mm, $Re = 574$)



(c) Falling film thickness ($\epsilon = 3.2$ $Re = 1104$)

Fig. 6 Reliability verification of model

time. The model was divided by the quadrilateral mesh to improve the mesh quality and calculate the film thickness accurately.

Figure 3 indicated that the mean film thickness is almost a constant data when the grid number of the model is greater than 51932. It is obvious that 51932 is an appropriate number of grids, so the following simulation was carried out in the condition of 51932 grid number. In the same principle, the proper grid number of other tubes are obtained.

Time step is also a crucial factor which affects the accuracy of simulation result. The following time steps were used

to perform the validation of time step independence: 0.005, 0.01, 0.02, 0.05 and 0.1 ms. Figure 4 reveals that the film thickness tends to be stable when the time step is less than 2×10^{-5} s. Thus, the final time step was chosen to be 2×10^{-5} s by many times of explorations and comparing the simulation data and experimental results.

2.6 Solution methods

According to previous literature and comparison of different simulation methods, the following solution methods are

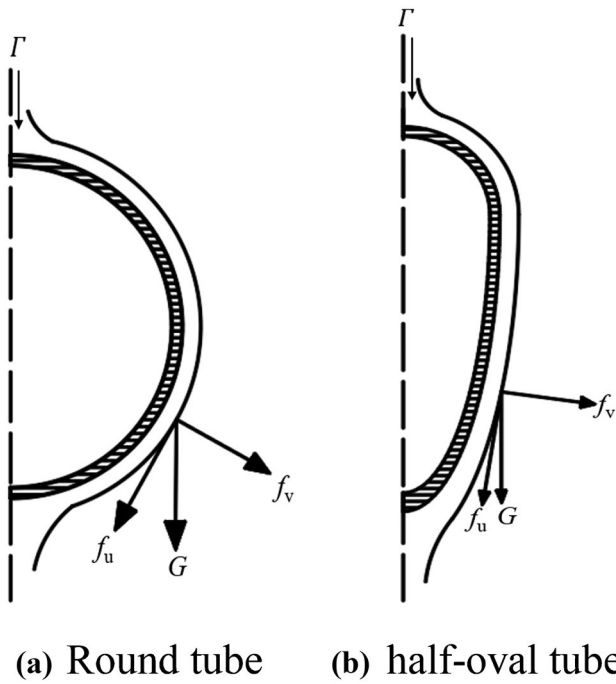


Fig. 7 The component force of gravity for different tube shape

adopted: PISO algorithm is applied for velocity–pressure coupling, which has a faster iteration speed. Pressure interpolation scheme utilizes Body Force Weighted model because gravity is considered in the simulation process. The spatial discretization of momentum and energy employ Second order upwind. Geo-Reconstruct method is used to capture the boundary of water film.

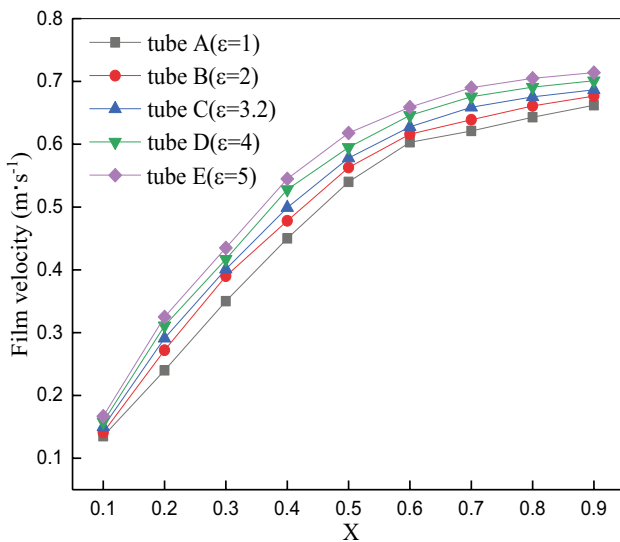


Fig. 8 Film velocity of different tube shape in circumferential direction (Re = 1104)

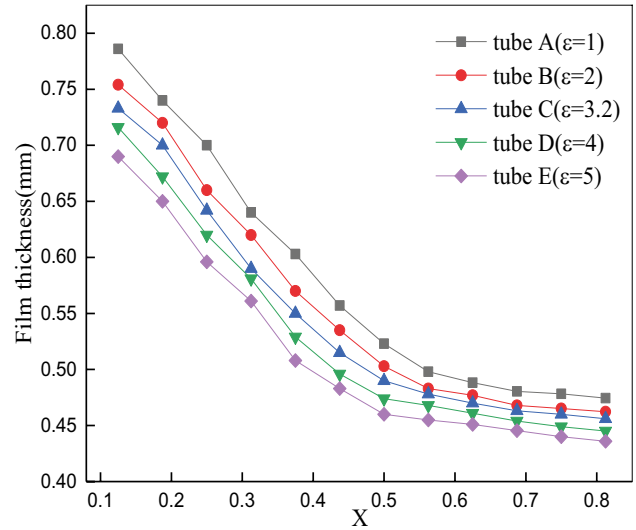


Fig. 9 Film thickness of different tube.

3 Model verification

The experimental platform was established to prove the reality of numerical model. Figure 5 presented the schematic diagram of experiment device. The experimental table contains three parts: the water circulation equipment, image acquisition system and measurement device of liquid film. The test tube was a horizontal half-oval tube ($\epsilon = 3.2$) which made of aluminum alloy. The test tube and distribution tube have the same length that is 150 mm. The distribution tube

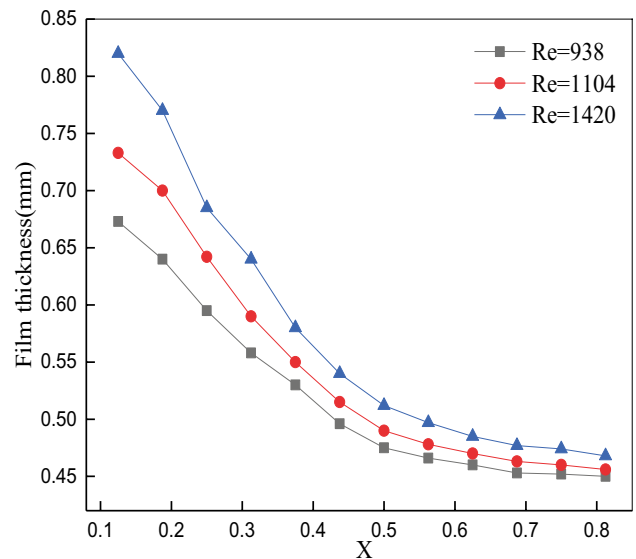


Fig. 10 Comparison of film thickness under shape in circumferential direction (Re = 1104) different Reynolds number ($\epsilon = 3.2$)

has a special structure to make sure the 7 spray holes whose radius is same with the simulation model have the equal spray density. To measure the film thickness with laser-induced fluorescence method, the dye of Rhodamine B with intense fluorescence was added into water. The dye can generate fluorescent light with a wavelength range of 578–610 nm when irradiates by green laser [28], Thus it is easy to distinguish the water film when take pictures through a filter. MATLAB is used to process all the photos. Parken calculated the mean heat transfer coefficient with a experiment in the condition of evaporation [19], which is similar with our simulation condition. The simulation model of circular tube whose diameter is 25.4 mm was built, the mean heat transfer coefficient under different Reynolds number and the film thickness in circumferential direction under the condition of $Re = 574$ were compared with experiment value in the paper of Parken et al. [19] and Zhao et al. [29], respectively. As illustrated in Figs. 5 and 6(a), (b), (c) the variation trend of falling film thickness and average heat transfer coefficient are similar with experimental value, and the difference of each point between simulation data and experimental values are within 9.8%.

4 Results and discussion

4.1 Velocity and liquid film thickness under different tube shape

The liquid film flows along the circumference in a combined function of gravity, surface tension, viscous force. As shown in Fig. 7 the component force of gravity in flow direction of half-oval tube is larger than that of round tube, which indicates that the liquid film has a greater acceleration when flows along the circumferential direction. And the component force of gravity is in proportion to ε , which means that the velocity of liquid film increases as the tube shape gets narrow and long. As illustrated in Figs. 6–8, the film velocity increases along the perimeter direction. The slope of the tangent line for film velocity curve gets smaller and smaller with X increasing. The film velocity gradually increases since water column collide tube surface because of the effects of gravity. Then several kinds of forces are almost balanced when circumferential dimensionless location is close to 1, so the film velocity is nearly a constant value. As ε increases, the component of gravity in flow direction increase, which leads to a increase in film velocity. The mean film velocity of tube B, C, D, E are approximately 4.5%, 7.6%, 11.2%, 14.5% greater than that of the round tube.

A larger velocity make the falling film is not easily accumulate on the tube wall. That is to say, a greater velocity indicates a thinner film thickness. As described in Figs. 7–9,

mean film thickness of tube B, C, D, E are about 3.7%, 6.3%, 8.6%, 11.4% lesser than that of the round tube respectively. The relationship between film thickness and Reynolds number is similar to the circular tube, Figs. 8–10 shows a larger Reynolds number also results in a thicker liquid film thickness on the half-oval tube.

4.2 Heat transfer performance under different tube shapes

The heat transfer coefficient of the five tubes for different circumferential dimensionless location are illustrated in Figs. 9–11. The variation tendency of heat transfer coefficient first obviously lower and gradually become stable along the perimeter direction. The heat transfer coefficient has a visible difference at top half of the tube wall, that phenomenon resembles the distribution of liquid film. The reason is that the impact of water column impingement is lager on the top area of the tube wall, the liquid film is strongly disturbed and thus has a larger heat transfer coefficient. For any one of the five tubes, heat transfer coefficient in the upper area play a dominate role in overall heat transfer performance. The local heat transfer coefficient is in direct proportion to ε . Contrasted with the circular tube, half-oval tube has a greater velocity and thinner film thickness, so it can improve the heat transfer performance. To be precise, the mean heat transfer coefficient over half-oval tube B, C, D, E are about 3.2%, 6.5%, 8.7%, 11.3% greater than that of the round tube respectively.

The dimensionless temperature θ is introduced to further understand the mechanism that heat transfer coefficient change with ε . The dimensionless temperature inside the liquid film is illustrated in Figs. 10–12(a), (b), (c), (d), (e). In all the five tubes, the dimensionless temperature

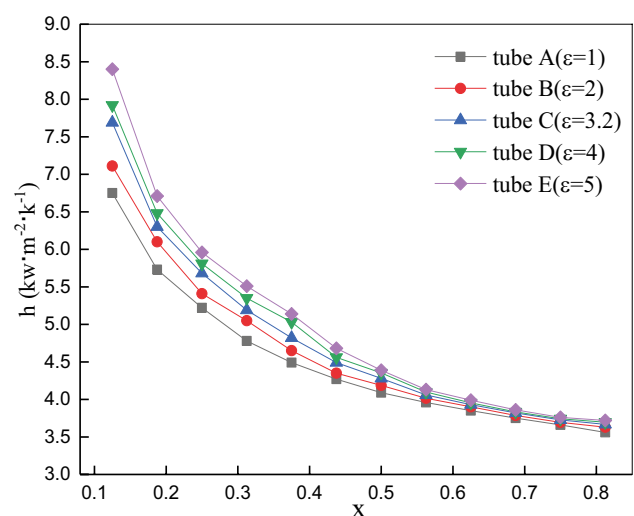


Fig. 11 Heat transfer coefficient for different tube shapes ($Re = 1104$)

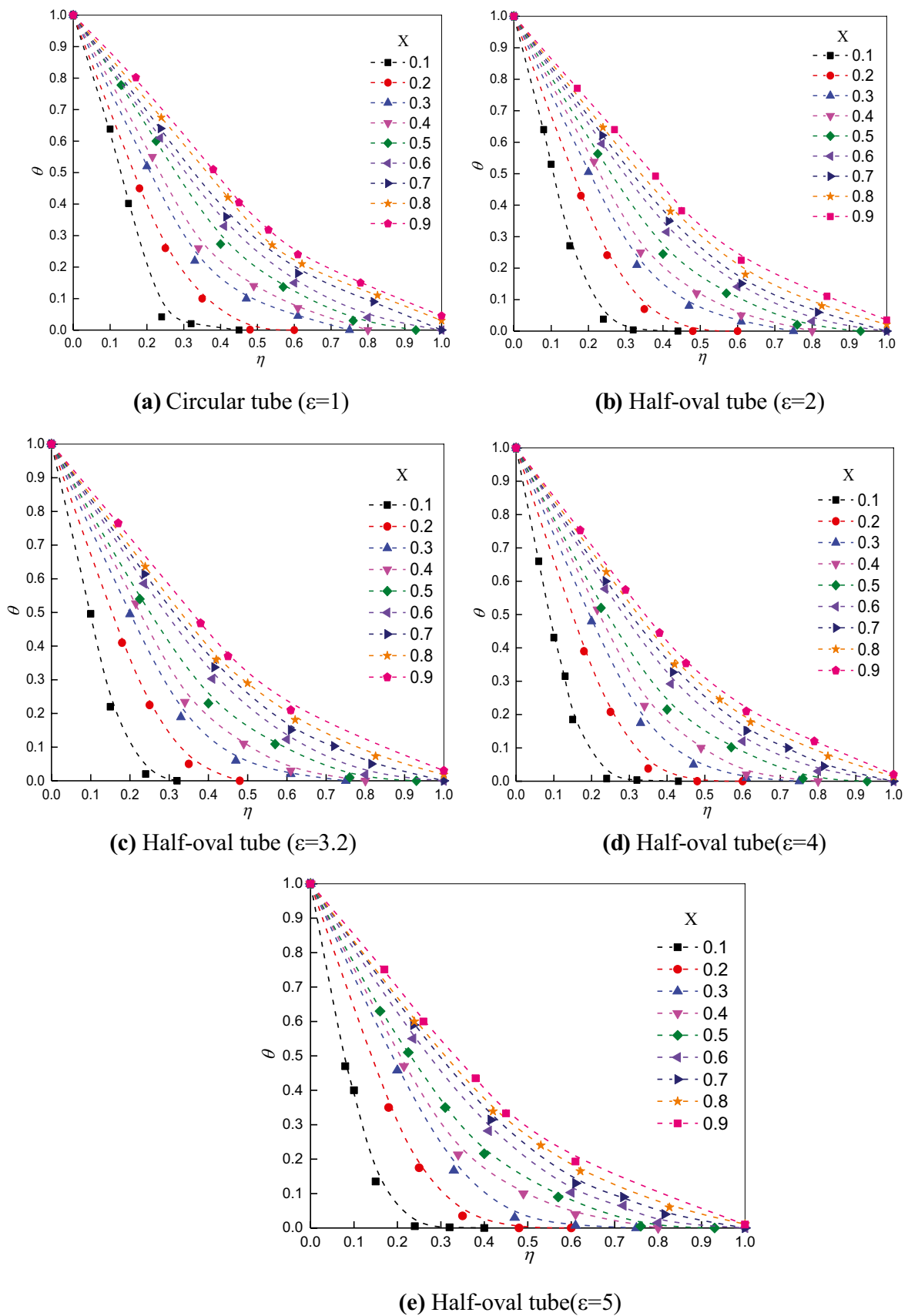
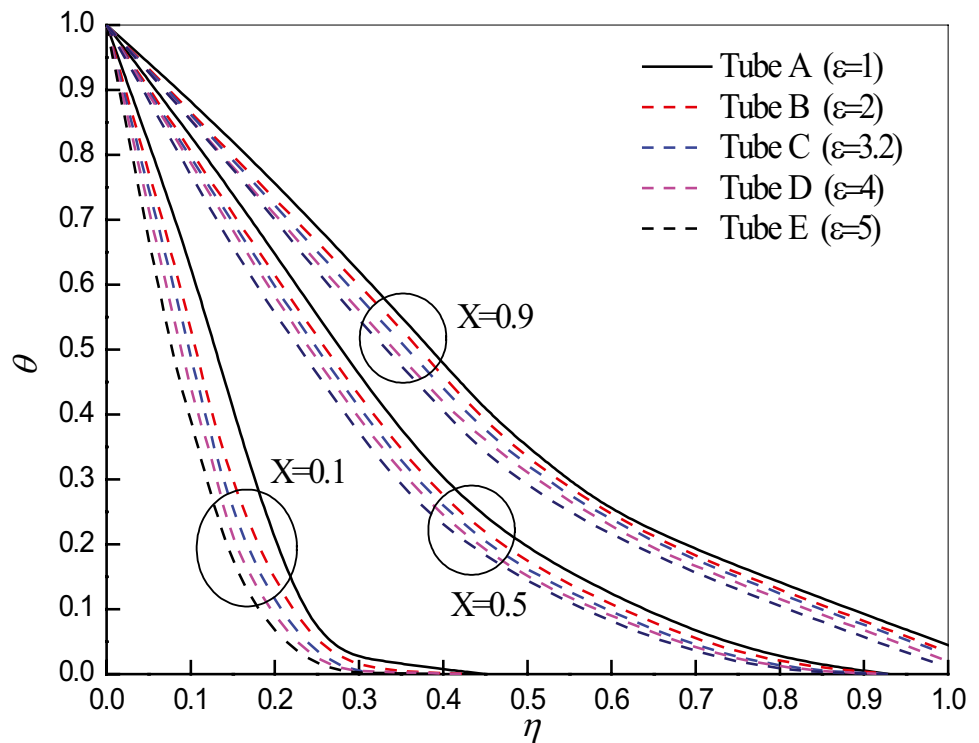


Fig. 12 Dimensionless temperature distribution of different tubes (Re=1104)

Fig. 13 Comparison of dimensionless temperature ($Re = 1104$)



gradually increases along the circumferential direction, it decreases faster in the upper part than that in the lower part, which indicates that the local temperature gradient gets smaller and thermal boundary layer becomes thicker along the perimeter direction. This means that local heat transfer performance gets worse and worse with the increase of circumferential angle.

The dimensionless temperatures of different tubes at 0.1, 0.5 and 0.9 circumferential dimensionless location are compared in Figs. 11–13. The dimensionless temperature distribution shows a similar trend at the three circumferential dimensionless location, the dimensionless temperature decreases with ϵ increasing. This further accounts for that half-oval tubes have a smaller thermal boundary layer and higher heat transfer efficiency than round tube A.

5 Conclusions

The falling film distribution and heat transfer performance over five tubes with the same perimeter and different shape was calculated by using a 2-D model. Half-oval tubes is better than round tube in film thickness, dimensionless temperature and heat transfer coefficient. The larger the ϵ , the more obvious the advantage of half-oval tube. According to the discussion and analysis above, it can be came to the following conclusions:

(1) The film thickness increases with Reynolds number increasing, and presents a variation trend that first rapidly decreases and then almost becomes stable in circumferential direction. The film thickness gradually decreases with ϵ from 1 to 5. The mean film thickness over half-oval tubes are approximately 3.7–11.4% lesser than that of circular tube.

(2) The mean film velocity of four half-oval tubes are nearly 4.5–14.5% higher than that of round tube.

(3) Local heat transfer coefficient gets smaller along the perimeter direction, and becomes larger and larger as ϵ increasing. The mean heat transfer coefficient over half-oval tube B, C, D, E are about 3.2%, 6.5%, 8.7%, 11.3% larger than that of round tube.

(4) In summary, Half-oval tube ($\epsilon = 5$) has the thinnest film thickness and largest heat transfer coefficient.

Declarations

Conflict of interest The authors declared that there is no conflict of interest.

References

- Ribatski G, Jacobi AM (2005) Falling-film evaporation on horizontal tubes - a critical review. *Internat J Refrige-Revue Internation Du Froid* 28(5):635–653

2. Cyklis P (2017) Industrial scale engineering estimation of the heat transfer in falling film juice evaporators. *Appl Therm Eng* 123:1365–1373
3. Qi C, Han X, Lv H et al (2018) Experimental study of heat transfer and scale formation of spiral grooved tube in the falling film distilled desalination[J]. *Int J Heat Mass Transf* 119:654–664
4. Xu L, Ge M R, Wang SC et al (2004) Heat-transfer film coefficients of falling film horizontal tube evaporators. *Desalination* 166(1–3SI):223–230
5. Shen S, Gong L, Liu H et al (2015) Characteristic study of steam maldistribution in horizontal-tube falling film evaporators. *Appl Therm Eng* 75(SI):635–647
6. Nusselt W (1916) Die oberflächenkondensation des wasserdampfes. *Z Ver Deutsch Ing* 60(3):541–546
7. Lin S, Liu X, Li X (2019) The spatial distribution of liquid film thickness outside the horizontal falling film tube. *Internatl J Heat and Mass Transf* 143:(118577)
8. Chen X, Shen S, Wang Y et al (2015) Measurement on falling film thickness distribution around horizontal tube with laser-induced fluorescence technology. *Int J Heat Mass Transf* 89:707–713
9. Hou H, Bi Q, Ma H et al (2012) Distribution characteristics of falling film thickness around a horizontal tube. *Desalination* 285:393–398
10. Xu L, Wang S C Wang Y X et al (2003) Flowing state in liquid films over horizontal tubes. *Desalination*, 156(PII S0011–9164(03)00332–11–3SI):101–107
11. Zhang Y, Wang D, Liu Y et al (2020) Distribution characteristics of falling film thickness around a horizontal corrugated tube. *Internatl J Heat Mass Transf* 154(119773)
12. Gstoehl D, Roques JF, Crisinel P et al (2004) Measurement of falling film thickness around a horizontal tube using a laser measurement technique. *Heat Transfer Eng* 25(8):28–34
13. Zhou Y, Cai Z, Ning Z et al (2017) Numerical simulation of double-phase coupled heat transfer process of horizontal-tube falling film evaporation. *Appl Therm Eng* 118:33–40
14. Wang J, Chen X, Lu T et al (2019) Three-dimensional film thickness distribution of horizontal tube falling film with column flow. *Appl Therm Eng* 154:140–149
15. Qiu Q, Zhang X, Quan S et al (2018) 3D numerical study of the liquid film distribution on the surface of a horizontal-tube falling-film evaporator. *Int J Heat Mass Transf* 124:943–952
16. Qiu Q, Meng C, Quan S et al (2017) 3-D simulation of flow behaviour and film distribution outside a horizontal tube. *Int J Heat Mass Transf* 107:1028–1034
17. Yan W, Pan C, Yang T et al (2019) Experimental study on fluid flow and heat transfer characteristics of falling film over tube bundle. *Int J Heat Mass Transf* 130:9–24
18. Li M, Lu Y, Zhang S et al (2016) A numerical study of effects of counter-current gas flow rate on local hydrodynamic characteristics of falling films over horizontal tubes. *Desalination* 383:68–80
19. Parken WH, Fletcher LS, Sernas V et al (1990) Heat-transfer through falling film evaporation and boiling on horizontal tubes. *J Heat Transfer-Transact Asme* 112(3):744–750
20. Pu L, Li Q, Shao X et al (2019) Effects of tube shape on flow and heat transfer characteristics in falling film evaporation. *Appl Therm Eng* 148:412–419
21. Li W, Wu X, Luo Z et al (2011) Falling water film evaporation on newly-designed enhanced tube bundles. *Int J Heat Mass Transf* 54(13–14):2990–2997
22. Qi C, Feng H, Lv H et al (2016) Numerical and experimental research on the heat transfer of seawater desalination with liquid film outside elliptical tube. *Int J Heat Mass Transf* 93:207–216
23. Ji W, Zhao C, Zhang D et al (2016) Effect of vapor flow on the falling film evaporation of R134a outside a horizontal tube bundle. *Int J Heat Mass Transf* 92:1171–1181
24. Zhao CY, Ji WT, Jin PH (2018) Hydrodynamic behaviors of the falling film flow on a horizontal tube and construction of new film thickness correlation. *Int J Heat Mass Transf* 119:564–576
25. Fadhil B, Wrobel LC, Jouhara H (2013) Numerical modelling of the temperature distribution in a two-phase closed thermosyphon. *Appl Therm Eng* 60(1–2):122–131
26. Brackbill JU, Kothe DB, Zemach C (1992) A continuum method for modeling surface-tension. *J Comput Phys* 100(2):335–354
27. Ouldhadda D, Idrissi AI, Asbik M (2002) Heat transfer in non-Newtonian falling liquid film on a horizontal circular cylinder. *Heat Mass Transf* 38(7–8):713–721
28. Arbeloa IL, Rohatgimukherjee KK (1986) Solvent effects on the photophysics of the molecular-forms of rhodamine-b internal-conversion mechanism. *Chem Phys Lett* 129(6):607–614
29. Zhou C, Ji W, Jin P et al (2018) Hydrodynamic behaviors of the falling film flow on a horizontal tube and construction of new film thickness correlation. *Int J Heat Mass Transf* 119:564–576

Publisher's Note Springer Nature remains neutral with regard to jurisdictional claims in published maps and institutional affiliations.